PHOTONICS Research

Flexoelectric-effect-based light waveguide liquid crystal display for transparent display

Yunho Shin,[1] Yingfei Jiang,[1] Qian Wang,[1] Ziyuan Zhou,[1] Guangkui Qin,[2] and Deng-Ke Yang[1,3,*]

[1]Materials Science Program, Advanced Materials and Liquid Crystal Institute, Kent State University, Kent, Ohio 44242, USA
[2]BOE Technology Group Co., Beijing, China
[3]Department of Physics, Kent State University, Kent, Ohio 44242, USA
*Corresponding author: dyang@kent.edu

Received 1 April 2021; accepted 3 June 2021; posted 11 June 2021 (Doc. ID 426780); published 24 January 2022

We report a light waveguide liquid crystal display (LCD) based on the flexoelectric effect. The display consists of two parallel flat substrates with a layer of flexoelectric liquid crystal sandwiched between them. A light-emitting diode (LED) is installed on the edge of the display and the produced light is coupled into the display. When no voltage is applied, the liquid crystal is uniformly aligned and is transparent. The incident light propagates through the display by total internal reflection at the interface between the substrate and air, and no light comes out of the viewing side of the display. The display appears transparent. When a voltage is applied, the liquid crystal is switched to a micrometer-sized polydomain state due to flexoelectric interaction and becomes scattering. The incident light is deflected from the waveguide mode and comes out of the viewing side of the display. We achieved thin-film-transistor active matrix compatible driving voltage by doping liquid crystal dimers with large flexoelectric coefficients. The light waveguide LCD does not use polarizers as in conventional LCDs. It has an ultrahigh transmittance near 90% in the voltage-off state. It is very suitable for transparent display, which can be used for head-up display and augmented reality display.

https://doi.org/10.1364/PRJ.426780

1. INTRODUCTION

Transparent displays [1–7] have emerged as a class of next-generation optoelectronics with the development of smart devices and the Internet of Things (IoT) [8,9], such as smart windows [10–13], augmented reality (AR) displays [14–16], and head-up displays (HUDs) [17–19]. As a powerful medium, transparent display, showing visual information on transparent screens without affecting their original appearance and functionality, offers new opportunities to visually communicate. A number of different display technologies have developed to meet the growing demands of transparent displays, including the conventional liquid crystal display (LCD) [20–25], polymer network liquid crystal (PNLC) [26–28]/polymer dispersed liquid crystal display (PDLC) [29–32], organic light-emitting display (OLED) [33–36], mini/micro light-emitting display (mini/micro-LED) [37–39], and electrochromic display (EC) [40–42]. Among the types of displays, LCDs are still the leading technology in flat panel displays and are widely used in many applications due to their advantages such as high resolution, light weight, low manufacturing cost, and long lifespan. In a conventional LCD, light is produced by a backlight (or edgelight) source, which is usually light-emitting diodes (LEDs). The brightness of the pixels (display unit) of the display is controlled by the liquid crystal layer through the help of polarizers. Color images are displayed through the use of color filters. The polarizers and color filters absorb more than 90% of the light produced by the backlight, and therefore the energy efficiency of conventional LCDs is very low. When a conventional LCD with an edgelight is used for transparent display, the transmittance of the transparent state is less than 10%, which is undesirable.

An emerging liquid crystal display technology is the light waveguide liquid crystal display [43–47]. It consists of two parallel flat substrates with a layer of polymer stabilized liquid crystal sandwiched between them. The polymer stabilized liquid crystal is a composite of a liquid crystal and an anisotropic polymer network. An LED is installed on the edge of the display, and the produced light is coupled into the flat display system. When no voltage is applied, the liquid crystal is uniformly aligned and is transparent. The incident light bounces back and forth from the substrate–air interface due to total internal reflection (TIR), and it propagates through the display. No light comes out of the viewing side of the display. When a voltage is applied, the liquid crystal is switched into a micrometer-sized polydomain state due to the competition between the aligning effect of the applied voltage under dielectric interaction and the aligning effect of the dispersed polymer network. The liquid crystal becomes optically scattering. The incident light is scattered out of the waveguide propagation mode and comes

out of the viewing side of the display. The operation of this display does not need polarizers. Furthermore, it has an ultrafast submillisecond switching time, making it possible to show colored images by using a color sequential scheme. The transmittance of the transparent state (voltage-off state) is very high, near 90%, making it an excellent candidate for transparent display. There is, however, a problem with the polymer stabilized liquid crystal that it exhibits some residual light scattering due to the following two issues. First, it is difficult to perfectly match the refractive indices of the liquid crystal and polymer network. Second, once the liquid crystal is switched to the polydomain state under an applied voltage, it may not be able to relax to the initial orientation, even if the applied voltage is removed. The residual scattering does not much affect the transmittance of the voltage-off state, but it has a significant impact on the contrast ratio (CR) of the display, namely, the ratio between the brightness of the bright state (voltage-on state) and dark state (voltage-off state). The contrast ratio of light waveguide LCDs is usually less than 50:1.

In this paper we report a light waveguide LCD based on the flexoelectric effect. In this new display, there is no dispersed polymer. The light scattering polydomain state is produced by the flexoelectric effect. There is no residual scattering, and therefore the display has ultrahigh transmittance and high contrast ratio.

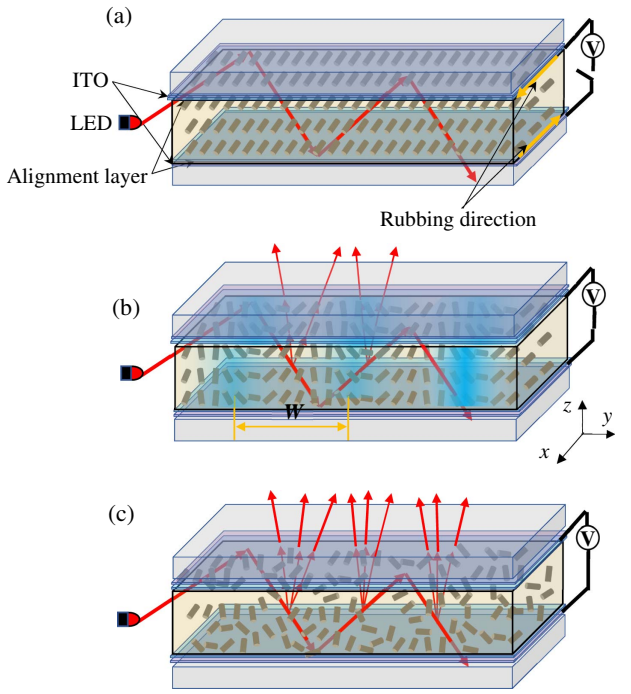

Fig. 1. Schematic diagram of the light waveguide LCD based on the flexoelectric effect. (a) Homogeneous state, (b) striped state, and (c) random polydomain state.

2. DISPLAY DESIGN AND OPERATION PRINCIPLE

The flexoelectric-based waveguide LCD is schematically shown in Fig. 1. It consists of two parallel glass substrates with a layer of liquid crystal (LC) sandwiched between them. On the inner surface of the substrate there is an indium-tin-oxide (ITO) coating, which serves as the transparent electrode. On top of the ITO there is a homogeneous alignment layer, which controls the orientation of the liquid crystal in the voltage-off state. The rubbing directions of the top and bottom alignment layer are antiparallel in the x direction. An LED is installed on the edge of the display where the top and bottom substrates are aligned. The driving circuitry is the other edge, which is orthogonal to the edge where the LED is installed.

When no voltage is applied, the LC is uniformly aligned along the rubbing direction—the x direction—of the alignment layer as shown in Fig. 1(a). The LC is transparent. The incident light propagates through the display under waveguide mode. No light comes out of the viewing side of the display.

When a voltage is applied across the cell in the z direction, there are two interactions between the LC and the applied electric field. The first one is the dielectric interaction, whose interaction energy is described by

$$f_{\text{dielectric}} = -\frac{1}{2}\Delta\varepsilon(\vec{E}\cdot\vec{n})^2, \tag{1}$$

where $\vec{E}$ is the applied electric field, $\vec{n}$ is the LC director (a unit vector along the average direction of the long molecular axis of the LC molecule), and $\Delta\varepsilon$ is the dielectric anisotropy of the LC. The dielectric interaction is not sensitive to the polarity of the applied voltage; specifically, when the voltage switches its polarity from positive to negative, its aligning effect on the LC is the same. If the constituent LC molecules have nonuniaxial cylindrical shape and a dipole; when the LC director is nonuniform spatially, namely, $\vec{n}$ varies in space, all the dipoles will point in a common direction. A net electric polarization is spontaneously produced, which is described by

$$\vec{P}_{\text{flexoelectric}} = e_s(\vec{n}\nabla\cdot\vec{n}) + e_b(\vec{n}\times\nabla\times\vec{n}), \tag{2}$$

where e_s and e_b are the splay flexoelectric and bend flexoelectric coefficients, respectively. $\nabla\cdot\vec{n}$ describes the splay deformation, and $\vec{n}\times\nabla\times\vec{n}$ describes the bend deformation of the LC director in space. Usually e_s is large when the LC molecule has a "pear" shape and has a permanent dipole parallel to the long molecular axis; e_b is large when the LC molecule has a "banana" shape and has a permanent dipole perpendicular to the long molecular axis. The polarization interacts with the applied electric field, called flexoelectric interaction, and the interaction energy is described by

$$\begin{aligned} f_{\text{flexoelectric}} &= -\vec{E}\cdot\vec{P}_{\text{flexoelectric}} \\ &= -[e_s(\vec{n}\nabla\cdot\vec{n}) + e_b(\vec{n}\times\nabla\times\vec{n})]\cdot\vec{E}. \end{aligned} \tag{3}$$

When the flexoelectric undulation occurs, on the one hand, the electric energy of the system is decreased. On the other hand, the elastic energy of the system is increased, which is described by

$$f_{\text{elastic}} = \frac{1}{2}K_{11}(\nabla\cdot\vec{n})^2 + \frac{1}{2}K_{33}(\vec{n}\times\nabla\times\vec{n})^2. \tag{4}$$

For the LC used in our experiment, the dielectric anisotropy is small and the dielectric interaction is negligible. We consider

the reorientation of the LC under the flexoelectric interaction. As an approximation we also neglect the variation of the LC director in the z direction. In the absence of an applied voltage, the LC uniformly orients along the x direction, and the LC director is given by

$$\vec{n} = \vec{n}_o = \hat{x}. \tag{5}$$

When a voltage V is applied, the LC is switched to the striped structure as shown in Fig. 1(b), where the LC director is given by [48]

$$\begin{aligned}\vec{n} &= \sqrt{1-\delta^2}\hat{x} + \delta \sin(ky)\hat{y} + \delta \cos(ky)\hat{z} \\ &= \hat{x} + \delta \sin(ky)\hat{y} + \delta \cos(ky)\hat{z},\end{aligned} \tag{6}$$

where δ is the amplitude and k is the wave vector of the flexoelectric undulation. Here, as an approximation, we consider the case where the amplitude δ of the undulation is small and only keep up to second-order terms of δ in the calculation of free energy. The applied electric field $\vec{E}$ is in the z direction. $\vec{E} = E\hat{z} = (V/d)\hat{z}$, where d is the cell thickness. The flexoelectric interaction energy density is given by

$$\begin{aligned}f_{\text{flexoelectric}} &= -\vec{E}\cdot\vec{P}_{\text{flexoelectric}} \\ &= -e_s\delta^2 k\cos^2(ky)E - e_b\delta^2 k\sin^2(ky)E.\end{aligned} \tag{7}$$

If $e_s > 0$ and $e_b > 0$, when the applied electric field is in the $+\hat{z}$ direction, $k > 0$ (the LC director rotates counterclockwise for the viewer looking at the $-\hat{x}$ direction) to minimize the flexoelectric interaction energy; when the applied electric field is in the $-\hat{z}$ direction, $k < 0$ (the liquid crystal director rotates clockwise for the viewer looking at the $-\hat{x}$ direction). The elastic energy density is given by

$$\begin{aligned}f_{\text{elastic}} &= \frac{1}{2}K_{11}(\nabla\cdot\vec{n})^2 + \frac{1}{2}K_{33}(\vec{n}\times\nabla\cdot\vec{n})^2 \\ &= \frac{1}{2}K_{11}[\delta k\ \cos(ky)]^2.\end{aligned} \tag{8}$$

The average (averaged over one period in the y direction) free energy density is

$$\begin{aligned}\bar{f} &= < f_{\text{elastic}} + f_{\text{flexoelectric}} > \\ &= -\frac{1}{2}(e_s + e_b)\delta^2 kE + \frac{1}{4}K_{11}\delta^2 k^2.\end{aligned} \tag{9}$$

We minimize the average free energy density with respect to the wave vector k:

$$\frac{\partial\bar{f}}{\partial k} = -\frac{1}{2}(e_s + e_b)\delta^2 E + \frac{1}{2}K_{11}\delta^2 k = 0.$$

We get

$$k = \frac{(e_s + e_b)E}{K_{11}}. \tag{10}$$

The width of the stripe is

$$W = \frac{\pi}{k} = \frac{\pi K_{11}}{(e_s + e_b)E} = \frac{\pi K_{11} d}{(e_s + e_b)V}. \tag{11}$$

The width W of the flexoelectric stripe is inversely proportional to the applied voltage V. It is difficult to accurately control the physical parameters K_{11}, e_s, and e_b of the liquid crystal in advance. However, once the liquid crystal is fixed, the cell thickness and applied voltage can be accurately controlled to obtain a desired stripe width.

The direction of the splay-bend deformation is sensitive to the polarity of the applied voltage, which can be seen from Eq. (3). When a low-frequency AC voltage is applied and the applied voltage is low, the magnitude of the deformation is small; the splay-bend deformation switches between the up and down directions following the switch of the polarity of the applied voltage changes. The LC is in the periodic striped state as shown in Fig. 1(b) and becomes optically diffracting. Some of the incident light is diffracted out of the waveguide mode and comes out of the viewing side of the display. When the applied voltage is high, the amplitude of the splay-bend deformation becomes large and the direction of the deformation cannot follow the polarity of the applied voltage changes, and then the LC is switched to a polydomain structure as shown in Fig. 1(c). The LC becomes optically scattering. The incident light is scattered out of the waveguide mode and comes out of the viewing side of the display.

3. EXPERIMENT AND RESULTS

The display cell used in our experiment consists of two glass substrates with ITO coating. The inner surfaces of the substrates are coated with the alignment material PI2170 (Nissan Chemical Industries, Ltd.), which is baked and rubbed for homogeneous alignment of the liquid crystals. The cell thickness is controlled by 2 μm spacers.

In order to achieve low driving voltages, the liquid crystal should have large flexoelectric coefficients. As discussed in the previous section, LC molecules with a "pear" shape and a permanent dipole parallel to the long molecular axis usually have large splay flexoelectric coefficients, and LC molecules with a "banana" shape and a permanent dipole perpendicular to the long molecular axis have large bend flexoelectric coefficients. In the construction of the LC for the display, three important physical properties must be considered. First, the LC must have large flexoelectric coefficients. Second, the LC should have a small dielectric anisotropy, such that the flexoelectric interaction is dominant. Third, the LC must be in nematic phase at room temperature. In our experiment we used liquid crystal dimers CB7CB and CB9CB, whose chemical structure is shown in Fig. 2. They consist of two mesogenic groups at the two ends and a flexible hydrocarbon chain in the middle. Because the number of carbons in the hydrocarbon chain is odd, they have a bent shape. Furthermore, the mesogenic groups have a cyano group that has a permanent dipole.

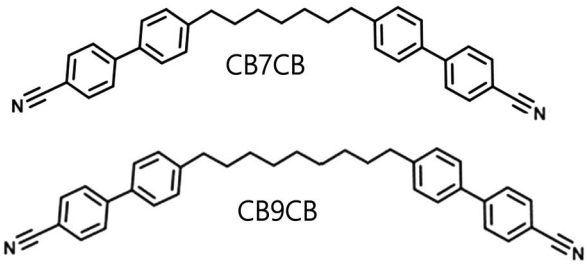

Fig. 2. Chemical structure of liquid crystal dimers CB7CB and CB9CB.

These dimers have large flexoelectric coefficients. The flexoelectric coefficient of CB7CB is −31 pC/m [49,50]. The flexoelectric coefficient of CB9CB is expected to be about the same. CB7CB transforms from isotropic phase to nematic phase at 114°C and from nematic phase to twist-bend nematic phase at 101°C [51]. CB9CB transforms from isotropic phase to nematic phase at 121°C and from nematic phase to twist-bend nematic phase at 105°C [52]. For display applications, the LC must be in nematic phase at room temperature. In order to decrease the transition temperature, we used regular nematic liquid crystals MAT978 and ZLI4330 (both from Merck). When only CB7CB (or CB9CB) is used, its phase separates from the regular LCs at a low concentration, which limits the maximum concentration of the dimer and thus limits the flexoelectric coefficient. Therefore, we used the two LC dimers to achieve a large flexoelectric coefficient. The dielectric anisotropies of CB7CB and CB9CB are about +2 [51]. The dielectric anisotropy of MAT978 is −4.0. The dielectric anisotropy of ZLI is −1.9. These two nematic LCs not only decrease the transition temperature but also keep the dielectric anisotropy small. Based on the above considerations, we developed an LC mixture consisting of 10% (mass fraction) nematic liquid crystal MAT 978, 50% nematic liquid crystal ZLI 4330, 25% liquid crystal dimer CB7CB, and 15% liquid crystal dimer CB9CB, which has the desired physical properties. The isotropic-nematic phase transition temperature of the LC (mixture) is 84°C. It was filled into the cell by capillary action in the isotropic phase at an elevated temperature. It is in the nematic phase at room temperature (around 22°C). All the measurements were performed at room temperature.

The response of the sample to applied voltages was studied under a Nikon polarizing optical microscope. The results are shown in Fig. 3. When the applied voltage is below 5.2 V (the threshold voltage), the LC remains in the homogeneous state. The polarizer is parallel to the alignment layer rubbing direction. The polarization of the incident light is parallel to the LC. When it propagates through the LC, its polarization remains unchanged. It is then absorbed by the analyzer. The sample appears black as shown in Fig. 3(a). When the applied voltage is increased above the threshold voltage, the splay-bend stripes start to form. At 8 V, the amplitude of the undulation is small, and the stripes are barely observable as shown in Fig. 3(b). As the applied voltage is increased more, the amplitude of the undulation increases. At 10 V, the stripes can be clearly observed as shown in Fig. 3(c). When the applied voltage is increased further, the width of the stripes becomes narrower and the stripes start to wiggle as shown in Fig. 3(d) where the applied voltage is 11 V. When the applied voltage is increased to 15 V, the stripes are broken into multiple domains as shown in Fig. 3(e).

The display was then studied under room light as shown in Fig. 4(a). A black absorbing layer was placed beneath the display to increase the contrast. The frequency of the applied voltage is 30 Hz. When no voltage is applied, the LC is in the homogeneous state. The sample does not reflect light and appears black as shown in Fig. 4(b). When the applied voltage is 10 V, the periodic splay-bend stripes are formed. The LC forms a grating, due to the periodic variation of the refractive index,

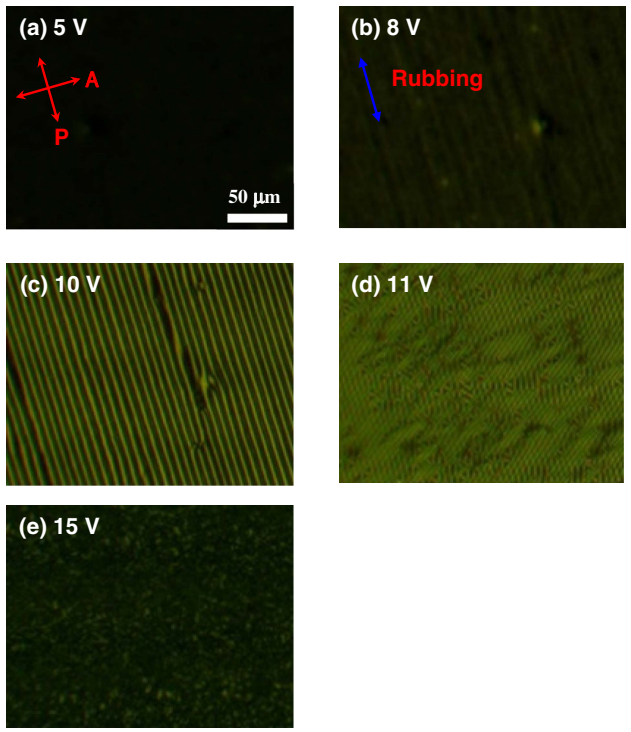

Fig. 3. Polarizing optical microphotographs of the waveguide LCD under various applied voltages. The frequency of the applied voltage is 30 Hz.

which diffracts light. The sample becomes colorful as shown in Fig. 4(c). When light is diffracted from different parts of the sample, the diffraction angles are different. Therefore, different parts of the sample exhibit different colors. When the applied voltage is varied in the region between 10 and 13 V, the stripe width decreases with increasing voltage, and the color of the light diffracted from the sample changes as shown in Figs. 4(d) and 4(e). When the applied voltage is increased to 15 V, the LC is switched to the polydomain state and the periodicity is lost.

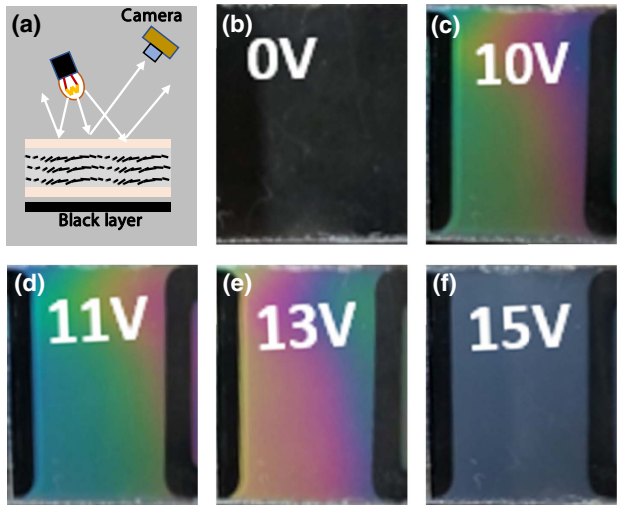

Fig. 4. Photographs of the waveguide LCD under various applied voltages. The frequency of the applied voltage is 30 Hz.

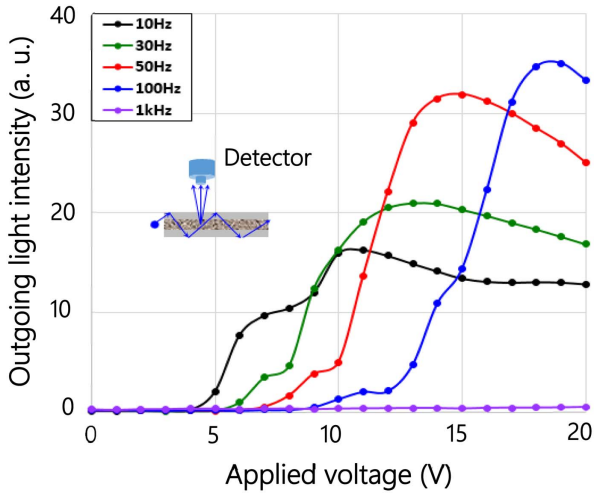

Fig. 5. Outgoing light intensity of the waveguide display versus applied voltage with different frequencies.

The LC scatters light, which is wavelength independent. Therefore, the sample appears white as shown in Fig. 4(f).

The electro-optical property was then measured. In the experiment, a white LED was installed on the edge of the display perpendicular to the alignment layer rubbing direction. The incident light propagates in the direction parallel to the rubbing direction. The light intensity coming out of the viewing side of the display was measured as a function of applied voltage. The result is shown in Fig. 5 (see Dataset 1, Ref. [53]). The outgoing light intensity depends on both the amplitude and frequency of the applied voltage. We first consider the voltage dependence. When the frequency of the applied voltage is 30 Hz, the light intensity versus voltage curve is shown by the red line. When the applied voltage is below 5 V (the threshold voltage), the light intensity is almost 0, indicating that the LC is in the homogeneous state and does not diffract or scatter light. When the applied voltage is increased above 5 V, the light intensity increases with the voltage, where first the LC diffracts light and then scatters light. When the voltage is 13 V, the maximum light intensity is reached. Beyond that, the light intensity decreases with the voltage. The decrease of the light intensity at high voltages is probably caused by the aligning effect of dielectric interaction on the LC. Because of the negative dielectric anisotropy of the LC, the dielectric interaction tries to align the LC parallel to the cell substrate. As shown by Eqs. (1) and (3), the dielectric interaction is proportional to the square of the applied electric field, while the flexoelectric interaction is linearly proportional to the electric field. At low voltages, the flexoelectric interaction is dominant; at high voltages, the dielectric interaction is dominant.

Now we consider the frequency dependence. When the frequency is low, the driving voltage is low, and the maximum light intensity is also low. When the frequency is increased, the maximum light intensity increases, and the driving voltage also increases. The increase of the threshold voltage with the frequency is not well understood at this moment. The increase of the light intensity with the frequency is caused by the dynamic behavior of the reorientation of the liquid crystal, which will be discussed in detail in the next paragraph. The optimum frequency is about 50 Hz, where the maximum light intensity is high. The contrast ratio between the outgoing light intensities of the bright state and dark state is high, about 184:1. The threshold voltage is 7 V, and the driving voltage (saturation voltage) for the maximum light intensity is 15 V. The difference between the saturation voltage and threshold voltage is 8 V, which is suitable for thin-film-transistor active matrix driving. Furthermore, in LCD driving, the voltage is alternated between a positive voltage and a negative voltage with the same amplitude in each picture frame. The picture frame time is usually in the range from 10 to 20 ms, corresponding to the frequencies of 100 Hz and 50 Hz, respectively. When the frequency of the applied voltage is 1 kHz, the outgoing light intensity is 0 and does not change with the applied voltage, due to the limited reorienting time of the LC. At this high frequency, the LC cannot rotate to follow the temporal variation of the voltage.

We studied the dynamic response of the waveguide display. In the study, an AC square voltage pulse is applied. The frequency of the voltage is 50 Hz, and the amplitude of the voltage is 15 V. The width of the pulse is 300 ms. The outgoing light intensity as a function of time is shown in Fig. 6 (see Dataset 2, Ref. [54]). When the voltage is turned on, the rising time is 3 ms. When the voltage is turned off, the falling time is 15 ms. During the pulse, the light intensity flickers with a frequency of 100 Hz, twice the frequency of the voltage. When the polarity of the applied voltage is switched, the light intensity increases first, and then decreases, because the aligning effect on the LC under the flexoelectric interaction is sensitive to the polarity of the voltage. When the polarity is switched, the splay-bend deformation tries to change direction, and many defects of the LC director are produced. The LC is in an irregular polydomain state, which scatters light strongly. Therefore, during the first part of the subframe, the outgoing light increases with time. The irregular polydomain state has a high elastic energy and is unstable. The LC will relax to the regular periodic striped state, which is less scattering. Therefore, during the second part of the subframe, the outgoing light decreases with time. When the frequency is in the region where the LC can follow the polarity of the applied voltage, the higher the frequency, the

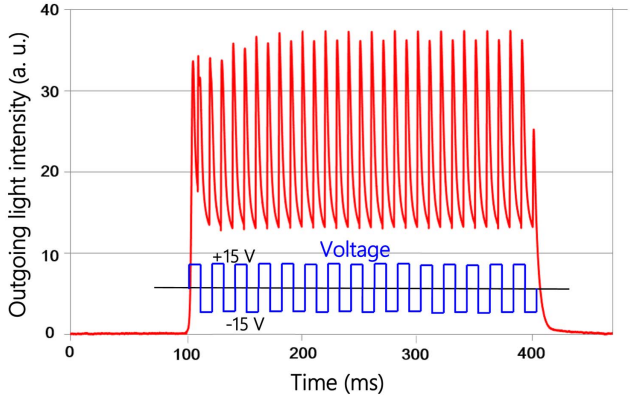

Fig. 6. Outgoing light intensity of the waveguide display versus time under 100 ms AC voltage pulse. The amplitude of voltage is 15 V, and the frequency of the voltage is 20 ms.

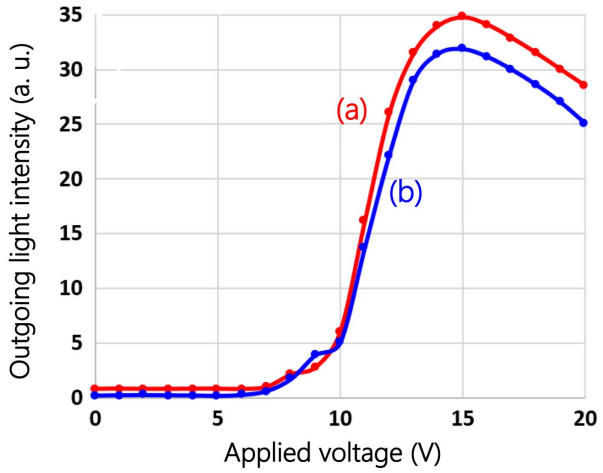

Fig. 7. Outgoing light intensity of the waveguide display versus applied voltage with the LED installed on different edges. (a) LED installed on the edge parallel to the stripe. (b) LED installed on the edge perpendicular to the stripe.

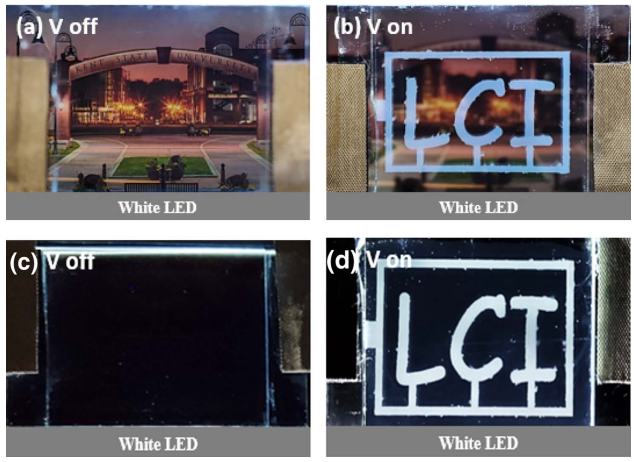

Fig. 8. Photographs of the waveguide display. (a) Transparent state in transparent display mode when applied voltage is 0. (b) Bright state in transparent display mode when applied voltage is 15 V. (c) Dark state in direct view display mode when applied voltage is 0. (d) Bright state in direct view display mode when applied voltage is 15 V.

percentage of time, when the liquid crystal is in the irregular poly-domain state, is larger, and therefore the outgoing light intensity is higher. When the frequency of the applied voltage is higher than 30 Hz, flickering is not observable to the human eye. Note that the light intensity reported in Fig. 5 is the time-average light intensity.

The electro-optical property of the waveguide display also depends on the incident light propagation direction with respect to the direction of the flexoelectric stripe, which is controlled by the rubbing direction of the alignment layer. The flexoelectric stripe is parallel to the rubbing direction of the alignment layer. In the measurement of the outgoing light intensity presented in Figs. 5 and 6, the LED is installed on the edge perpendicular to the alignment layer rubbing direction. We made another display where the LED is installed on the edge parallel to the rubbing direction. The result is shown by curve (a) in Fig. 7. For comparison, the result for the display where the LED is installed on the edge perpendicular to the rubbing direction is shown by curve (b) in Fig. 7. For the display with the LED installed on the edge parallel to the rubbing direction, the incident light propagates in directions more or less perpendicular to the flexoelectric stripe. When the incident light propagates through the LC, the encountered refractive index varies more, and therefore the maximum outgoing light intensity is higher. The trade-off is that the minimum outgoing light intensity in the voltage-off state is also higher, which causes the contrast ratio to decrease to 44:1. For the display with the LED installed on the edge perpendicular to the rubbing direction, the incident light propagates in directions more or less parallel to the flexoelectric stripe. When the incident light propagates through the LC, the encountered refractive index varies less, and therefore the maximum outgoing light intensity is lower. The minimum outgoing light intensity in the voltage-off state is also lower, resulting in a contrast ratio of 184:1.

We fabricated a flexoelectric waveguide display with ITO electrode patterned to display the characters of "LCI." The dimensions of the display are 2 inch × 1.5 inch. A white LED is installed on the edge of the display. The display can be operated in two display modes: transparent display and direct view display. When the display is used as a transparent display, a picture of the Kent State University campus is placed behind the display. When no voltage is applied, the LC throughout the display is in the transparent homogeneous state, the entire display is in the transparent state with a transmittance close to 90%, and the picture can be clearly seen as shown in Fig. 8(a). When 15 V is applied, the LC in the region covered by the patterned ITO is switched to the scattering state, and white "LCI" characters are displayed as shown in Fig. 8(b). When it is used as a direct view display, a black absorbing layer is placed behind the display to obtain a high contrast ratio. When no voltage is applied, no light comes out of the viewing side of the display, and the display appears black as shown in Fig. 8(c). When 15 V is applied, bright white "LCI" characters are displayed as shown in Fig. 8(d).

4. DISCUSSION AND CONCLUSION

Waveguide liquid crystal displays are based on light scattering and do not need polarizers. They have very high transmittance in the voltage-off state, which is a significant advantage over conventional LCDs where polarizers are needed. They are very suitable for transparent displays, which can be used for projection displays, AR displays, and HUDs for automobiles, trains, and airplanes.

There are two types of waveguide liquid crystal displays. The first type is based on polymer stabilized liquid crystal, where the scattering polydomain structure is caused by the dispersed polymer network. The second type is based on the flexoelectric effect reported in this paper. The first type has very fast switching time; both turn-on and turn-off times are in the submillisecond range, with which a color-sequential scheme can be used to display full color images. Its driving voltage is compatible with the amorphous silicon-based active matrix (AM) driving

method for multiplex pixel displays. However, it has a drawback that there is some residual scattering in the voltage-off state, caused by slight refractive index mismatch between the LC and the dispersed polymer network, which limits its contrast ratio. The second type uses a homogeneous LC, and there is almost no scattering in the voltage-off state, and thus the display has a very high contrast ratio. Its driving voltage is about the same as that of the first type. The disadvantage is its turn-off time, which is too slow for the color sequential scheme. A main reason responsible for the slow turn-off time is its viscosity. The dimers used to increase the flexoelectric coefficient are large molecules. Doping the dimers into the LC significantly increases the viscosity.

The light scattering in the flexoelectric effect based waveguide display depends on the polydomains formed under flexoelectric interaction. The scattering of one domain may change with time. In displays, the volume of a pixel is typically about 50 μm × 50 μm × 10 μm. The domain size is typically about 5 μm × 5 μm × 5 μm. There are about 200 domains in one pixel. The large number of domains in one pixel makes the average outgoing light intensity repeatable and not change with time.

There are other types of scattering liquid crystal technologies, such as dynamic scattering and polymer dispersed liquid crystal (PDLC). The dynamic scattering is based on electrohydrodynamic instability, where a high ion density is required. The ions decrease the resistivity and thus increase power consumption. Furthermore, they also cause electro-chemical reactions and thus cause a long-term instability problem. For PDLC, it is impossible to switch the material to a state that is transparent for the waveguided incident light by applying a voltage across the top and bottom electrodes. Therefore, both dynamic scattering and PDLC are not suitable for waveguide LCDs.

In summary, we developed a flexoelectric-effect-based liquid waveguide LCD. It has a very high transmittance, near 90%, in the voltage-off state. It also has a high contrast ratio. It is very suitable for transparent display applications.

Funding. BOE Technology Group Co.

Disclosures. The authors declare no conflicts of interest.

REFERENCES

1. J. F. Wager, "Transparent electronics," Science **300**, 1245–1246 (2003).
2. C. W. Hsu, B. Zhen, W. Qiu, O. Shapira, B. G. DeLacy, J. D. Joannopoulos, and M. Soljačić, "Transparent displays enabled by resonant nanoparticle scattering," Nat. Commun. **5**, 3152 (2014).
3. A. Moheghi, M. Kashima, Q. Qin, Y. Dong, and D.-K. Yang, "54.3: PSCT for switchable transparent liquid crystal displays," SID Symp. Dig. Tech. Pap. **46**, 817–820 (2015).
4. Y.-H. Shin, Y. Jin, N.-S. Oh, C.-W. Jeon, and S.-B. Kwon, "A normally transparent polymer dispersed liquid crystal developed by using a two-step UV exposure method for transparent flexible displays," Sci. Adv. Mater. **8**, 369–375 (2016).
5. C. Il Park, M. Seong, M. A. Kim, D. Kim, H. Jung, M. Cho, S. H. Lee, H. Lee, S. Min, J. Kim, M. Kim, J.-H. Park, S. Kwon, B. Kim, S. J. Kim, W. Park, J.-Y. Yang, S. Yoon, and I. Kang, "World's first large size 77-inch transparent flexible OLED display," J. Soc. Inf. Disp. **26**, 287–295 (2018).
6. S. H. Shin, B. Hwang, Z. J. Zhao, S. H. Jeon, J. Y. Jung, J. H. Lee, B. K. Ju, and J. H. Jeong, "Transparent displays utilizing nanopatterned quantum dot films," Sci. Rep. **8**, 2463 (2018).
7. J. Li, H. K. Bisoyi, J. Tian, J. Guo, and Q. Li, "Optically rewritable transparent liquid crystal displays enabled by light-driven chiral fluorescent molecular switches," Adv. Mater. **31**, 1807751 (2019).
8. Z. L. Wang, "Self-powered nanosensors and nanosystems," Adv. Mater. **24**, 280–285 (2012).
9. J. Gubbi, R. Buyya, S. Marusic, and M. Palaniswami, "Internet of Things (IoT): a vision, architectural elements, and future directions," Future Gener. Comput. Syst. **29**, 1645–1660 (2013).
10. H.-K. Kwon, K.-T. Lee, K. Hur, S. H. Moon, M. M. Quasim, T. D. Wilkinson, J.-Y. Han, H. Ko, I.-K. Han, B. Park, B. K. Min, B.-K. Ju, S. M. Morris, R. H. Friend, and D.-H. Ko, "Optically switchable smart windows with integrated photovoltaic devices," Adv. Energy Mater. **5**, 1401347 (2015).
11. H. Khandelwal, A. P. H. J. Schenning, and M. G. Debije, "Infrared regulating smart window based on organic materials," Adv. Energy Mater. **7**, 1602209 (2017).
12. D. Ge, E. Lee, L. Yang, Y. Cho, M. Li, D. S. Gianola, and S. Yang, "A robust smart window: reversibly switching from high transparency to angle-independent structural color display," Adv. Mater. **27**, 2489–2495 (2015).
13. Y. Jiang, Y. Shin, and D.-K. Yang, "Dual-mode switchable liquid-crystal window," Phys. Rev. Appl. **12**, 054037 (2019).
14. P. Milgram, H. Takemura, A. Utsumi, and F. Kishino, "Augmented reality: a class of displays on the reality-virtuality continuum," Proc. SPIE **2351**, 282–292 (1995).
15. H. Huang and H. Hua, "High-performance integral-imaging-based light field augmented reality display using freeform optics," Opt. Express **26**, 17578–17590 (2018).
16. R. Talukder, Y. H. Javed, and S.-T. Wu, "High performance LCD for augmented reality and virtual reality displays," Liq. Cryst. **46**, 920–929 (2019).
17. B.-W. Yang, "Head-up display for automobile," U.S. patent 5,615,023 (March 25, 1997).
18. S. Asakawa, H. Tsutsui, Y. Taketomi, and E. Okuda, "Head up display unit, liquid crystal display panel, and method of fabricating the liquid crystal display panel," U.S. Patent No. 5,892,598 (April 6, 1999).
19. M. Homan, "The use of optical waveguides in head up display (HUD) applications," Proc. SPIE **8736**, 87360E (2013).
20. P.-G. De Gennes and J. Prost, *The Physics of Liquid Crystals* (Oxford University, 1993), Vol. **83**.
21. L. M. Blinov and V. G. Chigrinov, *Electrooptic Effects in Liquid Crystal Materials* (Springer, 1996).
22. S. E. Hicks, S. P. Hurley, R. S. Zola, and D.-K. Yang, "Polymer stabilized VA mode liquid crystal display," J. Disp. Technol. **7**, 619–623 (2011).
23. D.-K. Yang, *Fundamentals of Liquid Crystal Devices* (Wiley, 2014).
24. X. Zhou, G. Qin, Y. Dong, and D.-K. Yang, "Fast switching and high-contrast polymer-stabilized IPS liquid crystal display," J. Soc. Inf. Disp. **23**, 333–338 (2015).
25. M. Kim, H. S. Jin, S. J. Lee, Y.-H. Shin, H. G. Ham, D.-K. Yang, P. J. Bos, J. H. Lee, and S. H. Lee, "Liquid crystals for superior electro-optic performance display device with power-saving mode," Adv. Opt. Mater. **6**, 1800022 (2018).
26. D.-K. Yang, "Polymer-stabilized liquid crystal displays," in *Progress in Liquid Crystal Science and Technology: In Honor of Shunsuke Kobayashi's 80th Birthday* (2013), pp. 597–628.
27. D. K. Yang, Y. Cui, H. Nemati, X. Zhou, and A. Moheghi, "Modeling aligning effect of polymer network in polymer stabilized nematic liquid crystals," J. Appl. Phys. **114**, 243515 (2013).
28. Y.-H. Shin, N.-S. Oh, and S.-B. Kwon, "Electro-optical properties of vertically aligned polymer network liquid crystals for normally transparent light shutters," Mol. Cryst. Liq. Cryst. **644**, 130–136 (2017).
29. J. W. Doane, A. Golemme, J. L. West, J. B. Whitehead, Jr., and B.-G. Wu, "Polymer dispersed liquid crystals for display application," Mol. Cryst. Liq. Cryst. **165**, 511–532 (1988).
30. N.-S. Oh, Y.-H. Shin, H.-Y. Kang, and S.-B. Kwon, "High performance dye-doped emulsion type PDLC for transmittance variable devices," Mol. Cryst. Liq. Cryst. **644**, 137–144 (2017).

31. Y.-H. Shin, N.-S. Oh, and S.-B. Kwon, "Electro-optical properties of normally transparent polymer dispersed liquid crystal cells with polymer wall and network structure," Mol. Cryst. Liq. Cryst. **647**, 415–421 (2017).
32. J. Jiang, G. McGraw, R. Ma, J. Brown, and D.-K. Yang, "Selective scattering polymer dispersed liquid crystal film for light enhancement of organic light emitting diode," Opt. Express **25**, 3327–3335 (2017).
33. H. Ochi, S. Fujimura, A. Yoshida, T. Miyadera, and M. Tsuchida, "Flexible OLED displays using plastic substrates," IEEE J. Sel. Top. Quantum Electron. **10**, 107–114 (2004).
34. B. Geffroy, R. P. Le, and C. Prat, "Organic light-emitting diode (OLED) technology: materials, devices and display technologies," Polym. Int. **55**, 572–582 (2006).
35. H. S. Shin, J. K. Jeong, Y. G. Mo, and D. U. Jin, "Organic light emitting display (OLED) and its method of fabrication," U.S. Patent No. 7,663,302 (February 16, 2010).
36. T. Tsujimura, *OLED Display Fundamentals and Applications* (Wiley, 2017).
37. H.-V. Han, H.-Y. Lin, C.-C. Lin, W.-C. Chong, J.-R. Li, K.-J. Chen, P. Yu, T.-M. Chen, H.-M. Chen, K.-M. Lau, and H.-C. Kuo, "Resonant-enhanced full-color emission of quantum-dot-based micro LED display technology," Opt. Express **23**, 32504–32515 (2015).
38. T. Wu, C. W. Sher, Y. Lin, C. F. Lee, S. Liang, Y. Lu, S. W. H. Chen, W. Guo, H.-C. Kuo, and Z. Chen, "Mini-LED and micro-LED: promising candidates for the next generation display technology," Appl. Sci. **8**, 1557 (2018).
39. Y. Huang, E. L. Hsiang, M. Y. Deng, and S. T. Wu, "Mini-LED, micro-LED and OLED displays: present status and future perspectives," Light Sci. Appl. **9**, 1 (2020).
40. C. G. Granqvist, A. Azens, A. Hjelm, L. Kullman, G. A. Niklasson, D. Rönnow, M. S. Mattsson, M. Veszelei, and G. Vaivars, "Recent advances in electrochromics for smart windows applications," Sol. Energy **63**, 199–216 (1998).
41. A. Azens and C. Granqvist, "Electrochromic smart windows: energy efficiency and device aspects," J. Solid State Electrochem. **7**, 64–68 (2003).
42. S. Lin, X. Bai, H. Wang, H. Wang, J. Song, K. Huang, C. Wang, N. Wang, B. Li, M. Lei, and H. Wu, "Roll-to-roll production of transparent silver-nanofiber-network electrodes for flexible electrochromic smart Windows," Adv. Mater. **29**, 1703238 (2017).
43. X. Zhou, G. Qin, L. Wang, Z. Chen, X. Xu, Y. Dong, A. Moheghi, and D.-K. Yang, "Full color waveguide liquid crystal display," Opt. Lett. **42**, 3706–3709 (2017).
44. L. Wang, N. Jia, L. Duan, T. Sun, Z. Liu, J. Fang, M. Hou, X. Liu, Y. Shi, Y. Li, X. Zhou, Y. Shin, G. Qin, S. Kim, X. Li, Y. Peng, S. Zhang, F. Yang, J. Sun, Q. Liu, B. Kristal, and D. Yan, "P-89: development of waveguide liquid crystal display for transparent display applications," SID Symp. Dig. Tech. Pap. **50**, 1573–1575 (2019).
45. C. Meng, E. Chen, L. Wang, S. Tang, M. Tseng, J. Guo, Y. Ye, Q. F. Yan, and H. Kwok, "Color-switchable liquid crystal smart window with multi-layered light guiding structures," Opt. Express **27**, 13098–13107 (2019).
46. Y. Shin, Q. Wang, G. Qin, and D.-K. Yang, "P-82: color flexible waveguide display using polymer stabilized liquid crystal," SID Symp. Dig. Tech. Pap. **51**, 1664–1667 (2020).
47. Y. Shin, J. Jiang, G. Qin, Q. Wang, Z. Zhou, and D.-K. Yang, "Patterned waveguide liquid crystal displays," RSC Adv. **10**, 41693–41702 (2020).
48. N. Éber, P. Salamon, and Á. Buka, "Electrically induced patterns in nematics and how to avoid them," Liq. Cryst. Rev. **4**, 101–134 (2016).
49. A. Varanytsia and L.-C. Chien, "Giant flexoelectro-optic effect with liquid crystal dimer CB7CB," Sci. Rep. **7**, 41333 (2017).
50. Y. Jiang, X. Zhou, Y. Shin, G. Qin, X. Xu, L. Zhou, S. Lee, and D.-K. Yang, "Image flickering reduction by dimer and polymer stabilization in FFS liquid crystal display," J. Soc. Inf. Disp. **27**, 285–294 (2019).
51. G. Babakhanova, Z. Parsouzi, S. Paladugu, H. Wang, Y. A. Nastishin, S. V. Shiyanovskii, S. Sprunt, and O. D. Lavrentovich, "Elastic and viscous properties of the nematic dimer CB7CB," Phys. Rev. E **96**, 062704 (2017).
52. R. J. Mandle, C. T. Archbold, J. P. Sarju, J. L. Andrews, and J. W. Goodby, "The dependency of nematic and twist-bend mesophase formation on bend angle," Sci. Rep. **6**, 36682 (2016).
53. D.-K. Yang, Y. Shin, Y. Jiang, Q. Wang, Q. Zhou, and G. Qin, "figure 5 and 7 data," figshare (2021), https://doi.org/10.6084/m9.figshare.14755341.
54. D.-K. Yang, Y. Shin, Y. Jiang, Q. Wang, Q. Zhou, and G. Qin, "figure 6 data," figshare (2021), https://doi.org/10.6084/m9.figshare.14755353.